Journal of Solid State Chemistry 187 (2012) 45–50

Contents lists available at SciVerse ScienceDirect

Journal of Solid State Chemistry

journal homepage: www.elsevier.com/locate/jssc

Synthesis, phase composition modification, and optical properties of Ce^{3+}/Tb^{3+} activated $KGdF_4$ and GdF_3 submicrocrystals

Chunyan Cao [a], Hyun Kyoung Yang [b], Byung Kee Moon [b], Byung Chun Choi [b], Jung Hyun Jeong [b,*], Kwang Ho Kim [c,*]

[a] College of Mathematics and Physics, Jinggangshan University, Ji'an 343009, PR China
[b] Department of Physics, Pukyong National University, Busan 608-737, South Korea
[c] School of Materials Science and Engineering, Pusan National University, Busan 609-735, South Korea

ARTICLE INFO

Article history:
Received 14 September 2011
Received in revised form
7 December 2011
Accepted 26 December 2011
Available online 3 January 2012

Keywords:
Synthesis
Phase composition modification
Optical properties
Energy transfer

ABSTRACT

Ce^{3+}/Tb^{3+} co-doped series of samples have been synthesized based on a citric acid assisted hydrothermal method. By controlling the hydrothermal treating time, the samples evolve from the Ce^{3+}/Tb^{3+} co-doped cubic phase $KGdF_4$ with spherical morphology into the Ce^{3+}/Tb^{3+} co-doped orthorhombic phase GdF_3 with rhombic shape finally. The X-ray diffraction data illustrate the phase composition modification process of the samples. The field emission scanning electron microscopy and the transmission electron microscopy images suggest the transformation in the morphology of final products. The spectra of the energy-dispersive spectroscopy reveal the constituents of the samples. And the selected area electronic diffraction patterns prove the crystalline phases of the samples. Based on previous studies and the experimental data, one possible phase composition modification process has been summarized. The photoluminescence excitation and emission spectra and the luminescent dynamic decay curves demonstrate the variations in optical properties of the Ce^{3+}/Tb^{3+} co-doped final products.

1. Introduction

Because of their practical and potential applications in phosphors, catalysts, and other functional materials as a result of their novel electronic, optical, and chemical properties arising from the 4*f* electrons, rare earth ions (RE^{3+}) doped materials have been extensively studied [1–4]. Fluorides are now receiving wide attention owing to the low frequency phonons usually observed in their crystal lattices [4,5]. The fluoride host materials with the composition $MGdF_4$, where *M* is Li, Na, or K, are of particular interest [6–8]. Recently, due to both its structural and optical properties, the RE^{3+} doped KF–GdF_3 system has received more attention [9–12]. In addition, Gd^{3+} is an ideal paramagnetic relaxation agent used in magnetic resonance imaging because of its large magnetic moment and nanosecond time scale electronic relaxation time [13,14]. Therefore, the RE^{3+} doped KF–GdF_3 system is very attractive when producing single-phase multifunctional materials.

Various synthetic strategies for the syntheses of reproducible and controllable materials have been developed by scientific researchers in last few decades. Due to their potential applications in biology and medicine, high quality (such as monodisperse, single-crystalline, well-shaped, and phase-pure) fluorides have been fabricated successfully. The hydrothermal treatment as a typical solution approach has been proven to be both effective and convenient in preparing various inorganic materials with diverse controllable morphologies and architectures [15]. In addition, the hydrothermal method is relatively simple, mild, and easy to produce a large amount of products, therefore, the hydrothermal route is often adopted to synthesize fluoride host materials. Materials synthesized through a hydrothermal method have a lot of factors to control, such as reaction time, reaction temperature, pH value, raw material, organic additive, etc. In the paper, we will study the effects of the reaction time on the structures, morphologies, and optical properties of the Ce^{3+}/Tb^{3+} co-doped final products based on the citric acid assisted hydrothermal method.

There have been few studies on the KF–GdF_3 system samples synthesized based on the hydrothermal method [10,12]. Moreover, the energy transfer (ET) from Ce^{3+} to Tb^{3+} has been investigated in many materials [16–19]. By lanthanide doping [20,21] or alkaline-earth doping [22], the researchers have

* Corresponding authors. Fax: +82 51 629 5549.
E-mail addresses: jhjeong@pknu.ac.kr (J.H. Jeong), kwhokim@pusan.ac.kr (K.H. Kim).

0022-4596/$ - see front matter © 2012 Elsevier Inc. All rights reserved.
doi:10.1016/j.jssc.2011.12.041

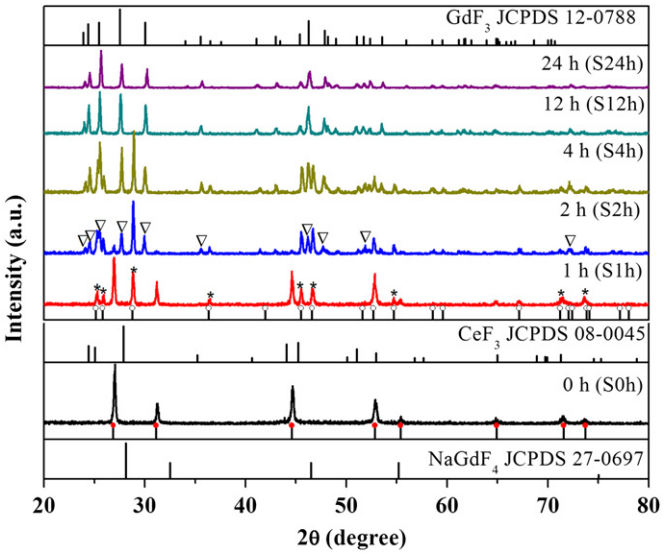

Fig. 1. Hydrothermal treating time dependent XRD patterns of final products and standard data of cubic phase $NaGdF_4$ (JCPDS 27-0697), hexagonal phase CeF_3 (JCPDS 08-0045), and orthorhombic phase GdF_3 (JCPDS 12-0788).

realized the phase transition or phase composition modification in some fluorides. In addition, some rhombic fluorides have been reported based on the thermal-decomposition procedure or the ionic liquid method [11,23–26]. To the best of our knowledge, there is no study on the synthesis of the rhombic shaped GdF_3 submicrocrystals which derive from the spherical $KGdF_4$ submicrocrystals. By controlling the hydrothermal treating time, we realize the phase composition modification from the Ce^{3+}/Tb^{3+} co-doped cubic phase $KGdF_4$ with spherical morphology into the Ce^{3+}/Tb^{3+} co-doped orthorhombic phase GdF_3 with rhombic shape based on a citric acid assisted hydrothermal method. Further, the optical properties of the obtained final products are compared and studied.

2. Experimental

2.1. Sample preparation

The samples were synthesized through a citric acid assisted hydrothermal method. The raw materials Gd_2O_3 (99.9%), Tb_2O_3 (99.99%), $Ce(NO_3)_3 \cdot 6H_2O$ (99.99%), KNO_3 (99.99%), citric acid (99.5+%), and NH_4F ($\geq$98%) were all purchased from Aldrich and used directly without further purification. The $Gd(NO_3)_3$ and $Tb(NO_3)_3$ solutions were prepared by dissolving the corresponding RE_2O_3 in nitric acid at elevated temperatures. In a typical synthesis procedure, 2 mmol of stoichiometric $RE(NO_3)_3$ (Gd^{3+}:Ce^{3+}:Tb^{3+}=85:10:5), 12 mmol of KNO_3, and 4 mmol of citric acid were dispersed into deionized water to form a 25 mL of clear solution by stirring. Then a 25 mL of aqueous solution that contained 12 mmol of NH_4F was introduced into the above solution. The pH value of the obtained turbid solution was 3 and then was adjusted to 1 by using dilute HNO_3. A 50 mL of the as-obtained turbid solution scaled by a measuring glass of plastics was transferred into a 70 mL of Teflon bottle held in a stainless steel autoclave, sealed, and maintained at 180 °C for 24 h. After the autoclave cooled down, the precipitates were collected by centrifugation, washed with ethanol and deionized water, and then dried in air at 60 °C for 24 h. The sample was denoted as S24h. In addition, the as-obtained solution was hydrothermal treated for 0 (collected directly), 1, 2, 4, and 12 h, and the corresponding obtained samples were signed as S0h, S1h, S2h, S4h, and S12h, respectively.

2.2. Characterization

The crystalline structures of the obtained samples were characterized by X-ray diffraction (XRD, Philips, Xpert/MPD) with Cu$K\alpha$ (λ=1.54056 Å) radiation. The 2θ ranges of all the datasets are from 20° to 80° with a step size of 0.02°. Field emission scanning electron microscopy (FE-SEM) and energy-dispersive spectroscopy (EDS) were taken on a JEOL JSM-6700F scanning electron microscope. Transmission electron microscopy (TEM) observation and selected area electronic diffraction (SAED) were performed with a JEOL JEM 2010 transmission electron microscope using an accelerating voltage of 200 kV. The room temperature photoluminescence (PL) excitation and emission spectra were recorded by using a Photon Technology International (PTI) fluorimeter with a Xe-arc lamp of power 60 W as excitation source. The luminescent dynamic decay curves of Tb^{3+} were measured by using a phosphorimeter attachment to the PTI with a Xe-flash lamp (25 W) as excitation source.

3. Results and discussion

3.1. Morphologies and structures

Fig. 1 presents XRD patterns of Ce^{3+}/Tb^{3+} co-doped hydrotheraml treating time dependent final products and standard JCPDS data. Similar to [10,12], the XRD data of the sample S0h (0 h) are similar to those of the cubic phase $NaGdF_4$ (a=5.52 Å, space group $Fm3m$ (2 2 5), JCPDS No. 27-0697) and the positions of diffraction peaks move toward lower angle for larger ionic radius of K^+ replacing Na^+, which means that the sample S0h is isostructural to that of the cubic phase $NaGdF_4$. Based on the assumption of the isostructure, a cubic unit cell with a=5.74 Å was obtained by employing the MDI JADE 5.0 software. The caculated diffraction peaks (red solid dot) are also plotted underside of the experimetnal pattern of sample S0h. After hydrothermal treated for 1 h (sample S1h), an unknown new material (marked as *) emerges besides $KGdF_4$. According to reflection peaks, the XRD pattern of the new material is similar to that of the hexagonal phase CeF_3 (a=7.11 Å, c=7.28 Å, space group $P6_3/mcm$ (1 9 3), JCPDS 08–0045) but the peak positions clearly move to higher angle. Similarly, a hexagonal unit cell with a=6.90 Å and c=7.08 Å were obtained and the caculated diffraction peaks (black hollow dot) are also plotted underside of the pattern of sample S1h. According to [20–22], if the dopant concentration is over 10%, this material should be called a solid solution. In the obtained new material, the concentration of GdF_3 maybe over 10%, so we believe that the new material should be a solid-solution of CeF_3–GdF_3–TbF_3. For the ionic radius of Gd^{3+} (Tb^{3+}) is smaller than that of Ce^{3+}, the diffraction peaks move toward higher angle. Another new material marked as ∇ emerges in sample S2h. This new material can be well indexed to the orthorhombic phase GdF_3 (space group $Pnma$ (62), JCPDS 12–0788). The $KGdF_4$ disappears in the sample S4h which is a mixture of the orthorhombic phase GdF_3 and the hexagonal phase solid solution of CeF_3–GdF_3–TbF_3. After hydrothermal treated for 12 h, pure orthorhombic phase GdF_3 is obtained. Increasing the hydrothermal time to 24 h (samples S24h) has no effect on the crystalline phase of the final product which is GdF_3 as well. The phase composition modification process of final products can be further proven by the FE-SEM, the EDS spectra, the TEM images, the SAED pattern, and the PL excitation and emission

spectra of the samples. And a possible phase composition modification process will be summarized in the context.

Fig. 2(a)–(f) depict the FE-SEM images of samples S0h, S1h, S2h, S4h, S12h, and S24h, respectively. Sample S0h are spherical particles with an average diameter of 200 nm and a rough surface. In addition to spherical particles, some hexagonal disks emerge in sample S1h, which is consistent with the above XRD data. Sample S2h are some spherical particles, some hexagonal disks with a length of about 400 nm and a height of about 100 nm, and a few smaller rhombic particles as well. Sample S4h are composed of some hexagonal disks and some rhombic particles, and the rhombic particles grow compared to those in sample S2h. After hydrothermal treated for 12 h, the particles are all in rhombic morphology with an average edge length of about 300 nm and a height of about 100 nm. Increasing the hydrothermal time to 24 h has little effect on the morphology of sample S24h which is also rhombic shaped. The morphology evolution is consistent well with the XRD patterns.

The samples are further characterized by TEM, SAED, and EDS. Fig. 3(a) and (b) show a TEM image and an EDS spectrum of sample S0h (cubic phase $KGdF_4$). The insets in Fig. 3(a) are a TEM image of one single spherical particle and a SAED pattern obtained from a single particle. The average size obtained from the TEM image is about 200 nm, which is consistent well with the data obtained from the FE-SEM image. The EDS spectrum suggests that the sample S0h is composed of Ce, Tb, F, Gd, and K. A TEM image and an EDS pattern of the sample S12h (GdF_3) are shown in Fig. 3(c) and (d), respectively. The insets in Fig. 3(c) are a single particle and a SAED pattern derived from a single particle. The EDS spectrum in Fig. 3(d) indicates that the sample S12h is composed of Ce, Tb, F, and Gd. As illustrated in Fig. 3, the TEM images suggest the difference in the morphologies of the two samples, the EDS patterns confirm the constituents of the two samples, and the SAED patterns prove the crystalline phase of the two samples.

As reported in [27,28], the strong acidic environment is propitious to form the GdF_3 samples. In our case, the pH value was adjusted after the $RE(NO_3)_3$ was introduced into the system. So the sample S0 maintained the cubic phase $KGdF_4$. The surfaces of the spherical particles were rough and even there were some amorphous particles in the sample. The rough surface was beneficial for the subsequent phase composition modification and morphology transformation. Based on previous studies [27–30] and the above data, we speculated that the phase composition modification from $KGdF_4$ to GdF_3 was related to a dissolution-reconstruction process in the strong acidic environment. Under high temperature and pressure, the corrosion (or the dissolving capacity) of the aqueous solution became stronger.

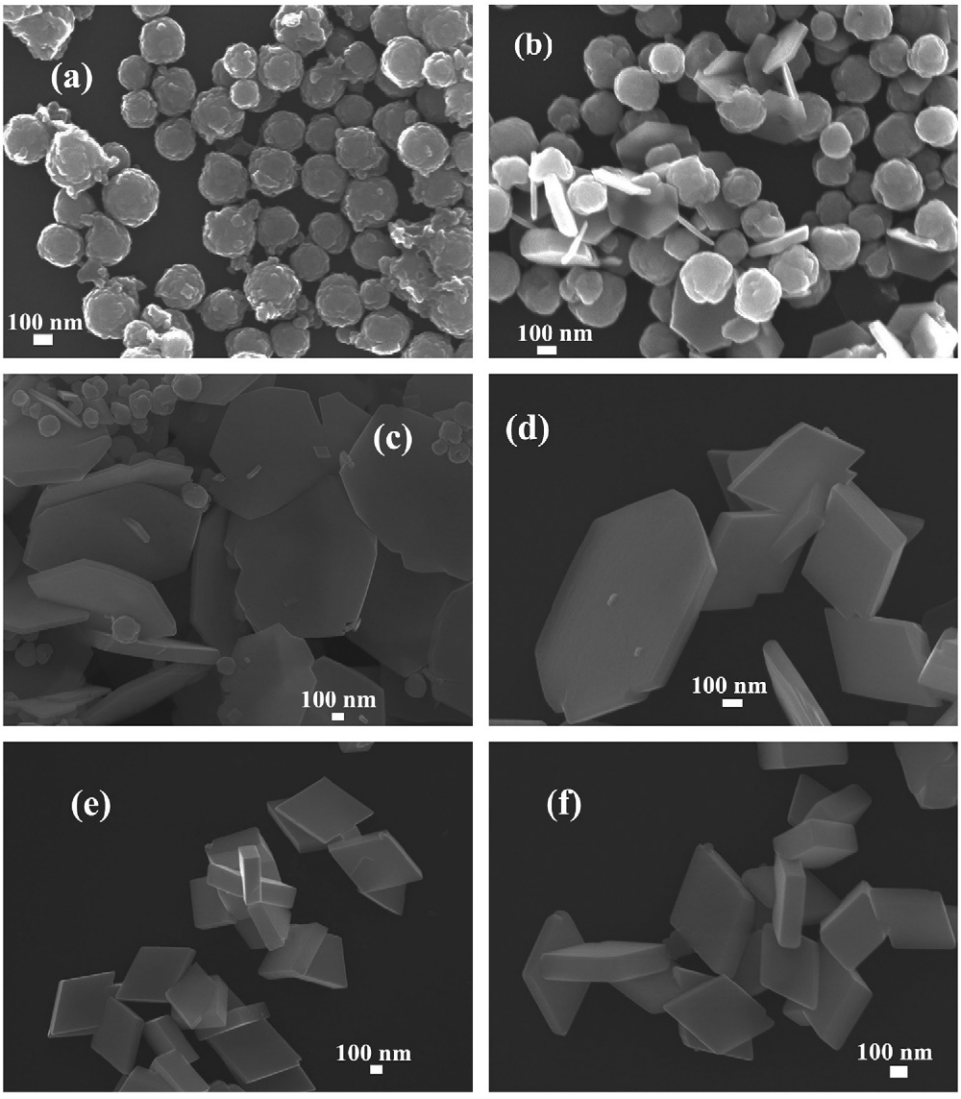

Fig. 2. FE-SEM images of samples (a) S0h, (b) S1h, (c) S2h, (d) S4h, (e) S12h, and (f) S24h.

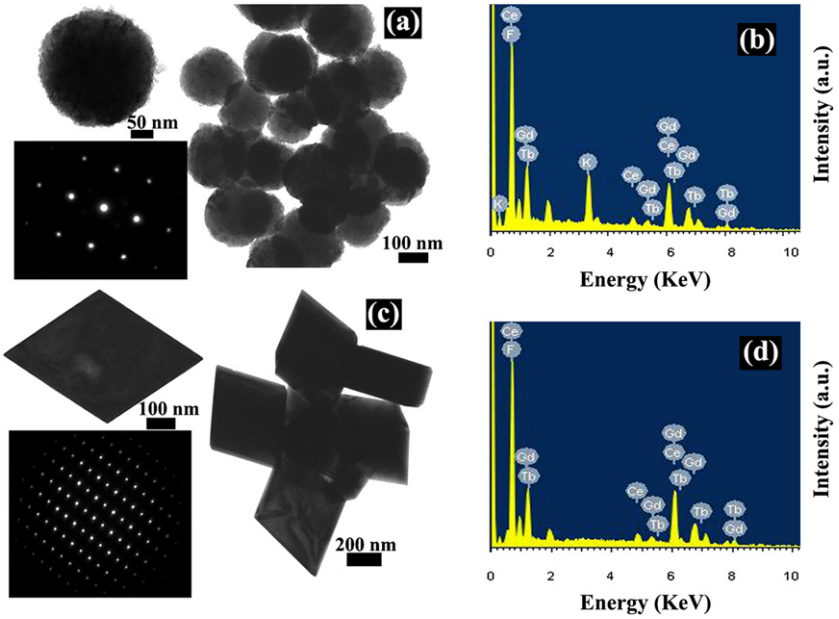

Fig. 3. TEM image (a) and EDS (b) of sample S0h ($KGdF_4$), TEM image (c) and EDS (d) of sample S12h (GdF_3). Insets in (a) and (c) are single particle and SAED pattern of the corresponding sample.

When the reaction time extended to 1 h, some Gd^{3+}, Ce^{3+}, and Tb^{3+} were released from Ce^{3+}/Tb^{3+} doped $KGdF_4$ in the solution and quickly reacted with the F^- to form the CeF_3–GdF_3–TbF_3 nuclei and subsequently grew into the hexagonal disk CeF_3–GdF_3–TbF_3 product. The obtained CeF_3–GdF_3–TbF_3 product exhibits the hexagonal phase as illustrated in the above text. With the reaction time increased to 2 h, more Gd^{3+}, Ce^{3+}, and Tb^{3+} were released. The concentration of Ce^{3+}/Tb^{3+} doped $KGdF_4$ decreased and the concentration of the CeF_3–GdF_3–TbF_3 increased. For the total concentration of Gd^{3+} was high in the raw material, the Ce^{3+}/Tb^{3+} doped orthorhombic phase GdF_3 emerged in the final products. With the reaction time increasing, the sample S4h became a mixture of the Ce^{3+}/Tb^{3+} doped GdF_3 and the CeF_3–GdF_3–TbF_3. The co-existence of the orthorhombic phase sample and the hexagonal phase sample may be caused by the gradual decrease of the basicity of the RE_2O_3 along the rare earth series, meaning that the formation of CeF_3 is easier than that of GdF_3 and TbF_3. The concrete reasons are under intensive study. When the reaction time increased to 12 h, the pure orthorhombic phase Ce^{3+}/Tb^{3+} doped GdF_3 was obtained. Extending the reaction time to 24 h, only the orthorhombic phase GdF_3 was obtained indicating that the Ce^{3+}/Tb^{3+}doped GdF_3 was stable in the strong acidic environment. The above XRD data, FE-SEM and TEM images, EDS spectra, and SAED patterns suggest the complexity of the phase evolution and the morphology transformation. For simplicity, a possible phase composition modification process of the samples is illustrated in Scheme 1. In the following, we will study the optical properties of the samples.

3.2. Photoluminescence properties

Fig. 4 illustrates the PL excitation spectra of final products. By monitoring at 544 or 544.5 nm emission of Tb^{3+}, the PL excitation spectra of the Ce^{3+}/Tb^{3+} co-doped final products present different properties. The Ce^{3+}/Tb^{3+} co-doped $KGdF_4$ (sample S0h) presents a broad excitation band peaking at 292.5 nm by monitoring at 544 nm emission of Tb^{3+}, which can be attributed to the electric dipole-allowed 4*f*–5*d* transition of Ce^{3+}. In addition, there are characteristic transitions of forbidden 4*f*–4*f* transitions within the Tb^{3+} configuration in the wavelength range of 320–

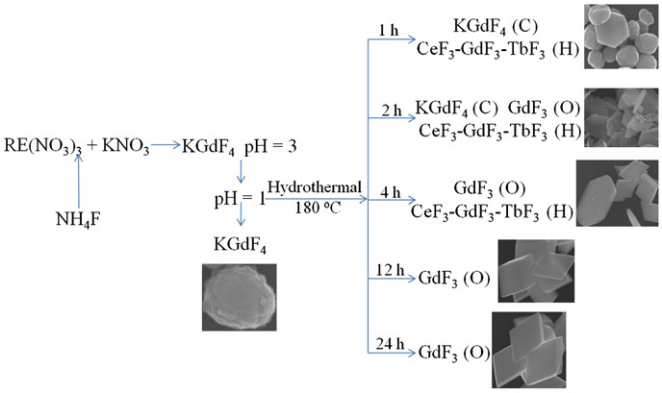

Scheme 1. Schematic illustration for phase composition modification from the Ce^{3+}/Tb^{3+} doped $KGdF_4$ to the Ce^{3+}/Tb^{3+}doped GdF_3 with multiform morphologies and different sizes. (C presents cubic phase, H presents hexagonal phase, and O presents orthorhombic phase.)

400 nm. The sample S1h presents the excitation band of Ce^{3+} with an inconspicuous shoulder in the short wavelength side. The excitation spectrum of sample S2h or S4h has a significant difference in the excitation band of Ce^{3+} to that of $KGdF_4$ (S0h). New excitation peaks at about 262 nm emerge while the band at 292.5 nm shifts to 288.5 nm. From the variation of intensities in the two bands, we can infer that the content of $KGdF_4$ decreases, which consists well with the XRD data. In addition, there are excitation peaks at around 274 and 312 (307) nm which can be assigned to the $^8S_{7/2} \rightarrow {}^6I_J$ and $^8S_{7/2} \rightarrow {}^6P_J$ transitions of host Gd^{3+}, respectively. The presence of Gd^{3+} excitation peaks in the PL excitation spectra indicates the existence of ET from Gd^{3+} to Tb^{3+}. For samples S12h and S24h, the excitation spectra of Ce^{3+} have only one main peak at about 263 nm. The disappearance of excitation band at 288.5 nm suggests the variations of located lattice environment around Ce^{3+} which indicates the phase composition modification of the final products. With the final products evolve from the Ce^{3+}/Tb^{3+} co-doped pure cubic phase $KGdF_4$, to a mixture of the cubic phase $KGdF_4$ and the solid solution CeF_3–GdF_3–TbF_3, to the Ce^{3+}/Tb^{3+} co-doped pure

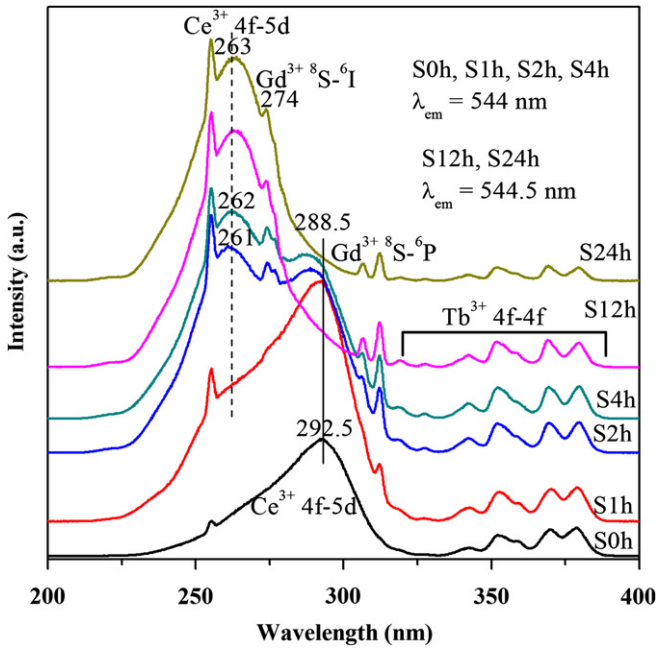

Fig. 4. Hydrothermal treating time dependent PL excitation spectra of final products.

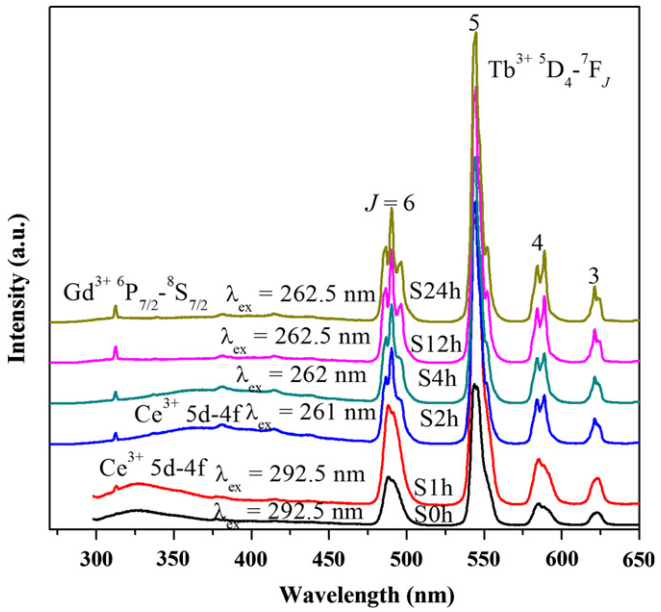

Fig. 5. Hydrothermal treating time dependent PL emission spectra of final products.

orthorhombic phase GdF_3, and the $4f$–$5d$ band of Ce^{3+} is sensitive to the host environment, the excitation bands of Ce^{3+} in the final products change greatly as illustrated Fig. 4. And the relative intensities of $4f$–$4f$ transitions of Tb^{3+} also change with the phase composition modification of final products.

With Ce^{3+} sensitization, PL emission spectra of the final products are illustrated in Fig. 5. The characteristic emission of Tb^{3+} $^5D_4 \rightarrow {}^7F_6$, $^5D_4 \rightarrow {}^7F_5$, $^5D_4 \rightarrow {}^7F_4$, and $^5D_4 \rightarrow {}^7F_3$ transitions are observed. As shown in Fig. 5, the splits of Tb^{3+} emissions become distinct with the phase composition modification of final products. The emission bands of Ce^{3+} $5d \rightarrow 4f$ are also very different in the final products as well. In the samples S0h and S1h, the emission bands of Ce^{3+} peak at about 328 nm, in the samples S2h and S4h, the emission bands of Ce^{3+} peak at about 365 nm, and in samples S12h and S24h, the Ce^{3+} has nearly no emission. In addition, there are emissions of Gd^{3+} $^6P_{7/2} \rightarrow {}^8S_{7/2}$ in the spectra. The appearance of Gd^{3+} emission indicates that the ET from Ce^{3+} to Gd^{3+} occurs. The emission of Gd^{3+} is much stronger in GdF_3 than that in $KGdF_4$ meaning that the ET from Ce^{3+} to Gd^{3+} is more efficient in GdF_3 than that in $KGdF_4$.

Fig. 6 displays the representative luminescent decay curves monitoring at the $^5D_4 \rightarrow {}^7F_5$ transition of Tb^{3+} in samples S0h ($KGdF_4$) and S24h (GdF_3). The decay curves can be well fitted by a single exponential function as $I(t)=I_0 \exp(-t/\tau)$, where I_0 is the initial emission intensity at $t=0$, τ is the $1/e$ lifetime of the $^5D_4$ level of Tb^{3+}. The lifetime in the Ce^{3+}/Tb^{3+} co-doped cubic phase $KGdF_4$ is 6.43 ± 0.03 ms, which is much longer than that in the Ce^{3+}/Tb^{3+} co-doped orthorhombic phase GdF_3 (5.01 ± 0.02 ms). The measurement conditions and the deduced lifetimes of the $^5D_4$ level of Tb^{3+} are listed in Table 1. The lifetime becomes shorter with the phase composition modification (hydrothermal time increasing) of final products except the sample S0h.

Based on previous studies of ETs in Ce^{3+}/Tb^{3+} co-doped gadolinium compounds [31,32] and the above PL excitation and emission spectra, we believe that the excitation energy is absorbed by Ce^{3+} $4f \rightarrow 5d$ transition and then mainly transferred to Tb^{3+} in the cubic phase $KGdF_4$ for the main excitation peak energy is lower than the ^6I_J levels of Gd^{3+}, and then the energy is released as visible emissions. In addition, Ce^{3+} can also transfer energy to Gd^{3+} then Gd^{3+} transfers the energy to Tb^{3+}. In the orthorhombic phase GdF_3 or the hexagonal phase CeF_3–GdF_3–TbF_3, the excitation energy is absorbed by Ce^{3+} $4f \rightarrow 5d$ transition and mainly transferred to Gd^{3+} for the energy levels match well and then Gd^{3+} transfer the energy to Tb^{3+}. Fig. 7 shows the schematic energy level diagram of Ce^{3+}, Tb^{3+}, and Gd^{3+} as well

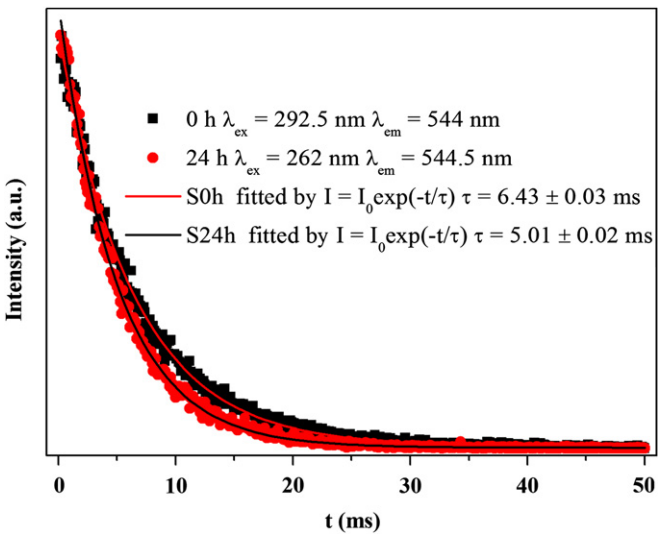

Fig. 6. Luminescent decay curves monitoring at the $^5D_4 \rightarrow {}^7F_5$ transition of Tb^{3+} in $KGdF_4$ (sample S0h) and GdF_3 (sample S24h).

Table 1
Spectroscopic parameters for $^5D_4 \rightarrow {}^7F_5$ lifetimes of Tb^{3+} in final products.

Sample	λ_{ex} (nm)	τ (ms)	Sample	λ_{ex} (nm)	τ (ms)
S0h	292.5	6.43 ± 0.03	S4h	262	6.18 ± 0.03
S1h	292.5	7.12 ± 0.04	S12h	262	5.27 ± 0.03
S2h	290	6.75 ± 0.03	S24h	262	5.01 ± 0.02
	262	6.21 ± 0.03			

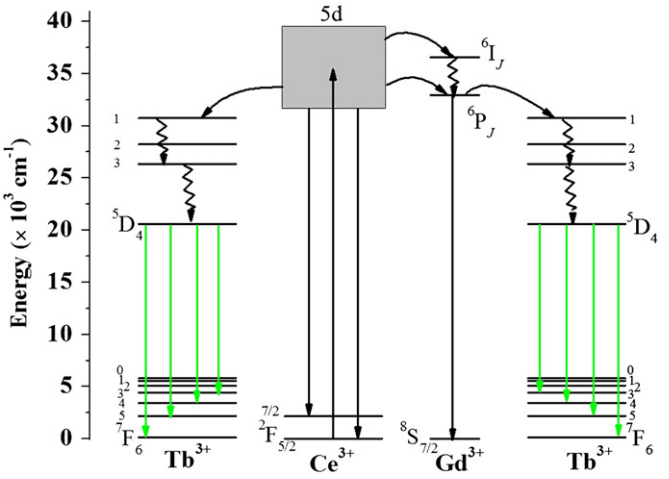

Fig. 7. Energy level diagram of Ce^{3+}, Tb^{3+}, Gd^{3+}, and possible excitation and emission processes in Ce^{3+}/Tb^{3+} co-doped final products.

as possible excitation and emission processes are plotted in Fig. 7. It illustrates that the luminescent process starts with excitation of Ce^{3+} followed by ET process from Ce^{3+} to Tb^{3+} directly or to Gd^{3+} to Tb^{3+}, and then the energy is released by them.

4. Conclusion

In conclusion, through a citric acid assisted hydrothermal route, a Ce^{3+}/Tb^{3+} co-doped series of samples have been synthesized. The final products evolve from the Ce^{3+}/Tb^{3+} co-doped pure cubic phase $KGdF_4$ to a mixture of the Ce^{3+}/Tb^{3+} co-doped cubic phase $KGdF_4$ and a solid solution of hexagonal phase CeF_3–GdF_3–TbF_3 to a mixture of the Ce^{3+}/Tb^{3+} co-doped orthorhombic phase GdF_3 and a solid solution of hexagonal phase CeF_3–GdF_3–TbF_3 to the Ce^{3+}/Tb^{3+} co-doped pure orthorhombic phase GdF_3 finally by controlling the hydrothermal treating time. For the 4*f*–5*d* band of Ce^{3+} is sensitive to the local host environment, Ce^{3+} presents different excitation properties in sensitizing Tb^{3+} emission while has a great difference in its own emissions in final products. PL emissions of Tb^{3+} vary with the phase composition modification of the final products. Correspondingly, the luminescent decay lifetimes of Tb^{3+} in the final products change as well. The phase composition modification process maybe observed in other fluorides, and the corresponding research is under intensive investigation.

Acknowledgments

This research was supported by Basic Science Research Program through the National Research Foundation of Korea (NRF) funded by the Ministry of Education, Science and Technology (no. 2011-0031373) and also this research was supported by National Core Research Center (NCRC) program through the National Research Foundation of Korea funded by the Ministry of Education, Science and Technology (2010-0001-226). The first author thanked for the Project of Young Excellent Doctor (JZB11001) supported by Jinggangshan University, China.

References

[1] S.V. Eliseeva, J.C. Bünzli, Chem. Soc. Rev. 39 (2010) 189–227.
[2] C.F. Guo, J. Yu, X. Ding, M. Li, Z.Y. Ren, J.T. Bai, J. Electrochem. Soc. 158 (2011) J42–46.
[3] B.C. Cheng, Z.D. Zhang, Z.H. Han, Y.H. Xiao, S.J. Lei, CrystEngComm 13 (2011) 3545–3550.
[4] C.X. Li, J. Lin, J. Mater. Chem. 20 (2010) 6831–6847.
[5] G.F. Wang, Q. Peng, J. Solid State Chem. 184 (2011) 59–363.
[6] R.T. Wegh, H. Donker, K.D. Oskam, A. Meijerink, Science 283 (1999) 663–666.
[7] F.T. You, S.H. Huang, S.M. Liu, Y. Tao, J. Lumin. 110 (2004) 95–99.
[8] P. Ptacek, H. Schäfer, K. Kömpe, M. Haase, Adv. Funct. Mater. 17 (2007) 3843–3848.
[9] M.A. Gusowski, A. Gągor, M. Trzebiatowska-Gusowska, W. Ryba-Romanowski, J. Solid State Chem. 179 (2006) 3145–3150.
[10] L.W. Yang, Y.Y. Zhang, J.J. Li, Y. Li, J.X. Zhong, P.K. Chu, Nanoscale 2 (2010) 2805–2810.
[11] Y.-P. Du, Y.-W. Zhang, L.-D. Sun, C.-H. Yan, Dalton Trans. (2009) 8574–8581.
[12] C.Y. Cao, H.K. Yang, J.W. Chung, B.K. Moon, B.C. Choi, J.H. Jeong, K.H. Kim, J. Mater. Chem. 21 (2011) 10342–10347.
[13] R. Kumar, M. Nyk, T. Ohulchanskyy, C. Flask, P. Prasad, Adv. Funct. Mater. 19 (2009) 853–859.
[14] Y. Park, J. Kim, K. Lee, K. Jeon, H. Na, J. Yu, H. Kim, N. Lee, S. Choi, S. Baik, H. Kim, S. ParK, B. Park, Y. Kim, S. Lee, S. Yoon, I. Song, W. Moom, Y. Suh, T. Hyeon, Adv. Mater. 21 (2009) 4467–4471.
[15] J.H. Liang, Q. Peng, X. Wang, X. Zheng, R.J. Wang, X.P. Qiu, C.W. Nan, Y.D. Li, Inorg. Chem. 44 (2005) 9405–9415.
[16] N. Guo, Y.H. Song, H.P. You, G. Jia, M. Yang, K. Liu, Y.H. Zheng, Y.J. Huang, H.J. Zhang, Eur. J. Inorg. Chem. 2010 (2010) 4636–4642.
[17] X.S. Qu, H.K. Yang, J.W. Chung, B.K. Moon, B.C. Choi, J.H. Jeong, K.H. Kim, J. Solid State Chem. 184 (2011) 246–251.
[18] M.Y. Xie, L. Yu, H. He, X.F. Yu, J. Solid State Chem. 182 (2009) 597–601.
[19] H. Guo, H. Zhang, J.J. Li, F. Li, Opt. Express 18 (2010) 27257–27262.
[20] F. Wang, Y. Han, C.S. Lim, Y.H. Lu, J. Wang, J. Xu, H.Y. Chen, C. Zhang, M.H. Hong, X.G. Liu, Nature 463 (2010) 1061–1065.
[21] D.Q. Chen, Y.L. Yu, F. Huang, A.P. Yang, Y.S. Wang, J. Mater. Chem. 21 (2011) 6186–6192.
[22] D.Q. Chen, Y.L. Yu, F. Huang, Y.S. Wang, Chem. Commun. 47 (2011) 2601–2603.
[23] V. Mahalingam, F. Vetrone, R. Naccache, A. Speghini, J.A. Capobianco, Adv. Mater. 21 (2009) 4025–4028.
[24] V. Mahalingam, R. Naccache, F. Vetrone, J.A. Capobianco, Chem. Commun. 47 (2011) 3481–3483.
[25] N.O. Núñez, M. Ocaña, Nanotechnology 18 (2007) 455606.
[26] M. Quintanilla, N.O. Núñez, E. Cantelar, M. Ocaña, F. Cussó, Nanoscale 3 (2011) 1046–1052.
[27] C.X. Li, J. Yang, Z.W. Quan, P.P. Yang, D.Y. Kong, J. Lin, Chem. Mater. 19 (2007) 4933–4942.
[28] D.M. Yang, X.J. Kang, M.M. Shang, G.G. Li, C. peng, C.X. Li, J. Lin, Nanoscale 3 (2011) 2589–2595.
[29] F. Zhang, Y. Wan, T. Yu, F.Q. Zhang, Y.F. Shi, S.H. Xie, Y.G. Li, L. Xu, B. Tu, D.Y. Zhao, Angew. Chem. Int. Ed. 46 (2007) 7976–7979.
[30] J.W. Mullin, Crystallization, 3rd ed, Butterworth-Heinemann, Oxford, 1997.
[31] G. Blasse, Mater. Chem. Phys. 16 (1987) 201–236.
[32] C.X. Li, P.A. Ma, P.P. Yang, Z.H. Xu, G.G. Li, D.M. Yang, C. Peng, J. Lin, CrystEngComm 13 (2011) 1003–1013.